Journal of Molecular Modeling (2022) 28: 148
https://doi.org/10.1007/s00894-022-05147-2

ORIGINAL PAPER

Electronic sensors for alkali and alkaline earth cations based on Fullerene-C60 and silicon doped on C60 nanocages: a computational study

Akbar Hassanpour[1] · Mohammad Reza Poor Heravi[2] · Azadeh Khanmohammadi[2]

Received: 21 February 2022 / Accepted: 3 May 2022 / Published online: 13 May 2022
© The Author(s), under exclusive licence to Springer-Verlag GmbH Germany, part of Springer Nature 2022

Abstract
In this research, we have reported the electrical sensitivity of pristine C60 and silicon doped on C60 (SiC59) nanocages as sensors that can be used for detecting the presence of alkali (Li^+, Na^+, K^+) and alkaline earth (Be^{2+}, Mg^{2+}, Ca^{2+}) cations. The computations are carried out at the B3LYP level of theory with a 6-31G(d) basis set. The atoms in molecules (AIM) and natural bond orbital (NBO) analyses are performed to evaluate the intermolecular interactions between cations and nanocages. The physical properties of the selected complexes are also analyzed by the frontier molecular orbital, energy gap, electronegativity, chemical hardness, softness, and other quantities such as work function, number of transferred electron, and dipole moment. The results show that the adsorption process is exothermic and with increasing the charge of cations, the adsorption energies enhance. Our findings also reveal a decrease in the energy gap along with an increase in the electrical conductivity of the respective complexes. Finally, the density of state calculations is presented to confirm the obtained results.

Keywords Fullerene-C60 · Sensor · Alkali and alkaline earth cations · Nanocages · AIM

Introduction

Fullerenes are a significant group of molecules in which large numbers of carbon atoms are locked together in an almost spherical shape. They have a graphite-like structure, but instead of all hexagonal sections, they also contain pentagons of carbon atoms that form a sheet in the shape of a sphere, oval, or cylinder. Putting these pentagons and hexagons together is essential for forming a spherical structure. A fullerene must have exactly 12 five-sided faces to close it in a spherical shape, but the number of hexagonal faces can be very different. It is an interesting molecule due to its symmetrical structure and reactivity to a variety of reagents.

Buckminsterfullerene [1] is one type of fullerene. Its molecules are spherical and contain 60 carbon atoms (12 pentagons and 20 hexagons). The most stable and abundant fullerenes are C60 and C70. Therefore, most of the properties mentioned in the case of fullerenes are focused on these two types. In the C60 structure, the carbon atoms of wall have a hybridization between the π and σ orbitals. This is due to its spherical structure, which limits the conjugate π bonding among the carbon atoms. Hence, this phenomenon leads to high reactivity of C60 [2].

Among the various nanostructures, fullerenes have received a great deal of attention due to their unique properties, which has made them attractive in a wide range of purposes. Known biomedical applications for fullerenes include the design of high-performance MRI contrast agents, X-ray imaging contrast agents, and photodynamic therapy [3–9]. They may also be used for drug and gene delivery systems in the body, in lubricants, and as catalysts. Other applications of fullerenes are mainly in the electronics, nanotechnology, materials science, and solar cells [10–12]. The doping fullerene has also attracted a lot of interest for its exploration due to its exclusive assets. For example, the K and Rb doping with C60 (K_xC60 and Rb_xC60) causes these compounds to become superconductors [13–18]. In addition, the antibacterial activity [19], HIV-P inhibition [20], and photo cytotoxicity [21] are some of the potential applications of the C60 derivatives.

✉ Mohammad Reza Poor Heravi
mrheravi@pnu.ac.ir

[1] Department of Chemistry, Marand Branch, Islamic Azad University, Marand, Iran

[2] Department of Chemistry, Payame Noor University (PNU), P.O. Box 19395-4697, Tehran, Iran

Fullerenes are known as zero-dimensional closed-cage nanomaterials. Hence, the spherical shape of fullerene nanomaterials gives this nanomaterial a large surface area [22–25]. This feature is important for biosensors and sensor systems. Although fullerenes can be dissolved in a variety of solvents, surface modification is an effective way to use them for biosensor and sensor technology. The most useful characteristic of the double bonds formed by the carbon structure in fullerenes is that they can be modified because they are able to easily respond to chemical reactions. Due to its spherical structure and 30 double bonds, it has the capacity to form 30 bonds that need to be modified with various chemical agents [26].

The choice of C60 in this study is due to the fact that it is one of the most plentiful fullerenes which is owing to minimize the strain of related instability by reducing the π overlap at adjacent pentagons sites [27]. C60 is an effective acceptor component with high electron affinity for charge transfer. The significant influences of chemical adsorption of the cations on the electrical sensitivity of pristine C60 and SiC59 nanocages could be the basis of new generation of electronic sensor design. It is well known that the heteroatom substitution of foreign atoms can modify and enhance the selectivity and sensitivity of C60s due to the different interactions of dopant and adsorbed factors [28]. The doping of C60 with the Si atom could modify the electronic properties due to inducted distortions in the neighboring positions. It can also alter the charge transfer and modifies the mechanic, chemical, and optic properties of C60.

The adsorption of metal ions on nanostructure surfaces has been observed in several theoretical and experimental studies [29–41]. The purpose of this work is to evaluate the adsorption of the alkali and alkaline–earth metal cations ($M = Li^+$, Na^+, K^+, Be^{2+}, Mg^{2+}, Ca^{2+}) on the pristine C60 and SiC59 nanocages. The titled interactions are theoretically investigated in terms of geometry, energies, and electronic structures using density functional theory (DFT). The topological parameters and charge transfer interactions are evaluated by AIM and NBO analyses, respectively. The effect of adsorbed cations on the electronic properties of pristine C60 and SiC59 nanocages is evaluated by frontier molecular orbital, energy gap, and chemical hardness and softness. These results may be useful for further studies on functionalization of the pristine and modified C60 nanocage as a sensor for the new compounds or drugs.

Computational details

In this paper, the structure of SiC59 is obtained by replacing the C atom at the head of a pentagon ring with the Si atom (Fig. 1). The complete optimization of geometry and the calculation of properties on the pristine C60 and SiC59 surfaces with and without the metal cations of Be^{2+}, Mg^{2+}, Ca^{2+}, Li^+, Na^+, and K^+ are done using the B3LYP function [42, 43] combined with the standard 6-31G(d) basis set. B3LYP has been revealed to be a reliable and commonly used functional for the study of different nanostructures [44–53]. The quantum chemistry package GAMESS [54] has been used to carry out all these calculations. The adsorption energies (E_{ads}) of metal cations on the nanocages are determined by the following equations:

$$E_{ads} = E_{(M@C60)} - E_{(M)} - E_{(C60)} \quad (1)$$

$$E_{ads} = E_{(M@SiC59)} - E_{(M)} - E_{(SiC59)} \quad (2)$$

where $E_{(M@C60)}$ and $E_{(M@SiC59)}$ are the total energies of the metal cations adsorbed on the pristine C60 and SiC59 nanocages, and $E_{(C60)}$, $E_{(SiC59)}$, and $E_{(M)}$ are referred to the energies of an isolated pristine C60, SiC59, and the mentioned metal cations, respectively. The adsorption energies of complexes are corrected for basis set superposition error (BSSE) using the counterpoise correction scheme predetermined by Boys and Bernardi [55]. The atoms in molecules (AIM) theory of Bader [56] is applied to evaluate the nature of the intermolecular interactions by means of AIM 2000 software [57]. In this calculation, the B3LYP/6-31G(d) wave functions are used as input. The NBO analysis [58, 59] is also performed at the same level of theory in order to evaluate the natural electron configuration of adsorbing metal cations and the electron charge transfer between metal cations and nanocages. The GaussSum program [60] is applied to calculate the density of state (DOS) results and to get a more precise insight into the electronic properties of the analyzed structures. Finally, the quantum molecular descriptors of complexes such as softness (S), chemical hardness (η) [61], and electronegativity (χ) [62] are analyzed using the highest occupied molecular orbital (HOMO) and the lowest unoccupied molecular orbital (LUMO) energies.

Results and discussion

Molecular geometry and interaction energy

The complete optimization of geometry in the pristine C60 and SiC59 structures as well as metal cations adsorbed on pristine C60 (M@C60) and SiC59 (M@SiC59) nanocages ($M = Li^+$, Na^+, K^+, Be^{2+}, Mg^{2+}, and Ca^{2+}) are performed using the DFT calculations at the B3LYP level of theory with the 6-31G(d) basis set. Figures 1, 2, and 3 show a number of the structures considered in this study. In the C60 nanocage, the two typical bond lengths C–C and C = C are about 1.453 Å and 1.395 Å, respectively. The single bond

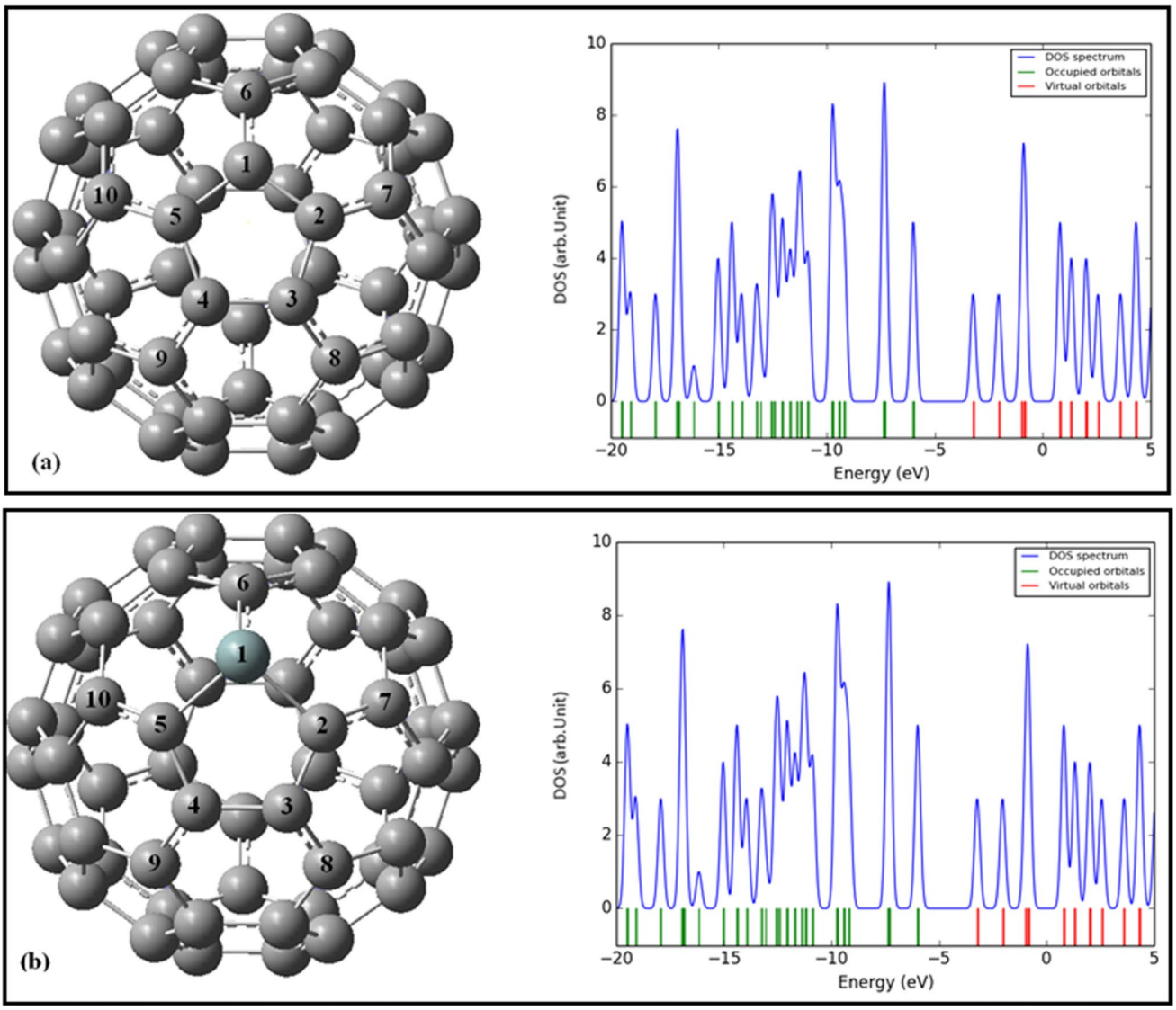

Fig. 1 The optimized structures and DOS plots of **a** fullerene C60 and **b** SiC59

exists between the pentagonal and hexagonal rings, whereas the double bond is present in the hexagonal rings.

Our findings also show that in the SiC59 nanocage, the bond lengths of C–C and C = C connected to the Si atom are 1.456 Å and 1.397 Å, respectively. These results are close to the same bonds in pristine C60 and do not change significantly. On the other hand, the calculations indicate that the C–Si–C angle in the SiC59 nanocage is 90.7°, which is less than the C–C–C angle with sp^3 hybridization (109.5°) in the C60 nanocage. When metal cations are adsorbed on the SiC59 nanocage, the C–Si–C angle for alkali and alkaline earth cations changes during the complexation. It can be expressed as Li^+ (88.3°), Na^+ (88.5°), K^+ (89.0°), Be^{2+} (83.6°), Mg^{2+} (86.9°), and Ca^{2+} (87.7°).

The adsorption energies (E_{ads}) of M@C60 and M@SiC59 are also computed to evaluate the stability of the considered complexes. The negative value of E_{ads} indicates the exothermic character of the adsorption process. Therefore, the addition of M cations leads to the formation of stable configurations. The theoretical results display that the alkaline earth cations increase the stability of all complexes more than the alkali ones. As shown in Table 1, E_{ads} is highly dependent on the nature of the different cations. For each ion group (alkali metal and alkaline earth), the calculations demonstrate that the E_{ads} values for the M@C60 and M@SiC59 complexes are approximately close to each other (see Table 1). Since these complexes are largely electrostatic in nature, it is easy to see that cations with higher charge density interact more strongly with nanocages. The data also show that the adsorption of alkaline earth cations on the SiC59 nanocage is stronger than the C60 one. However, the large values of E_{ads} denote that the

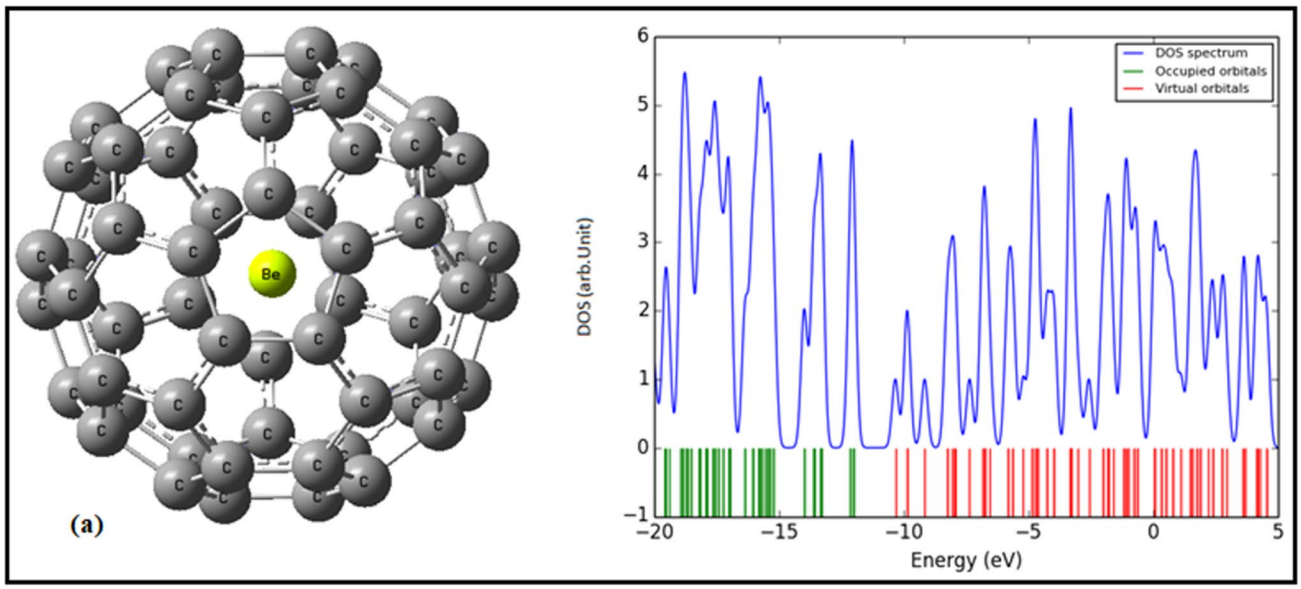
Be
(a)
DOS spectrum
Occupied orbitals
Virtual orbitals
DOS (arb.Unit)
Energy (eV)

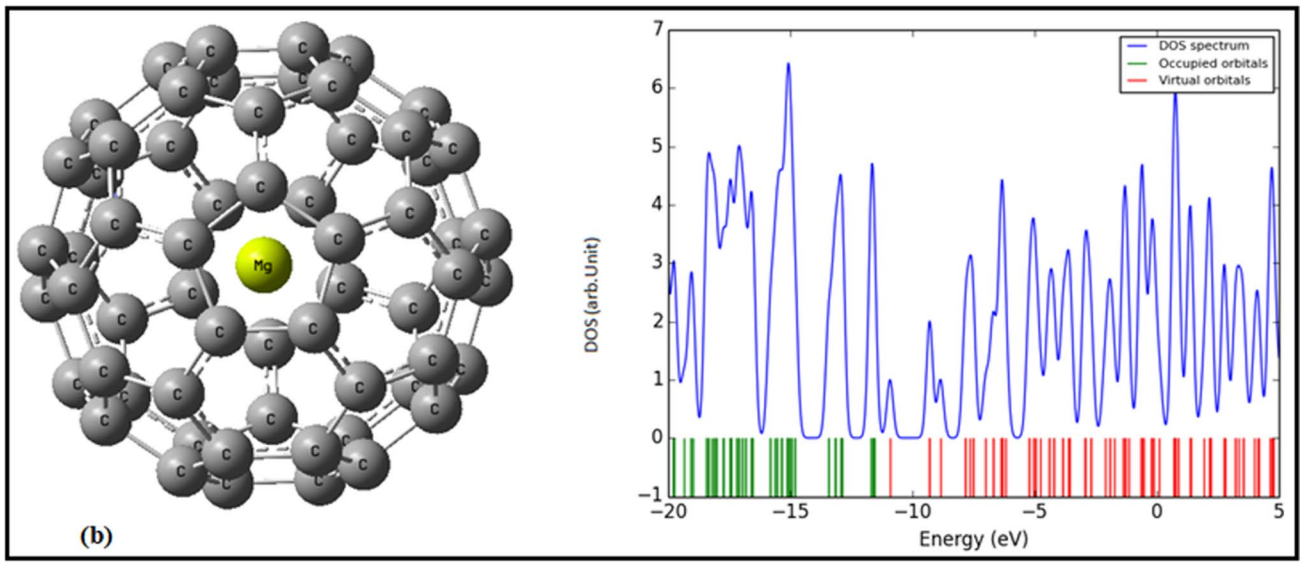
Mg
(b)
DOS spectrum
Occupied orbitals
Virtual orbitals
DOS (arb.Unit)
Energy (eV)

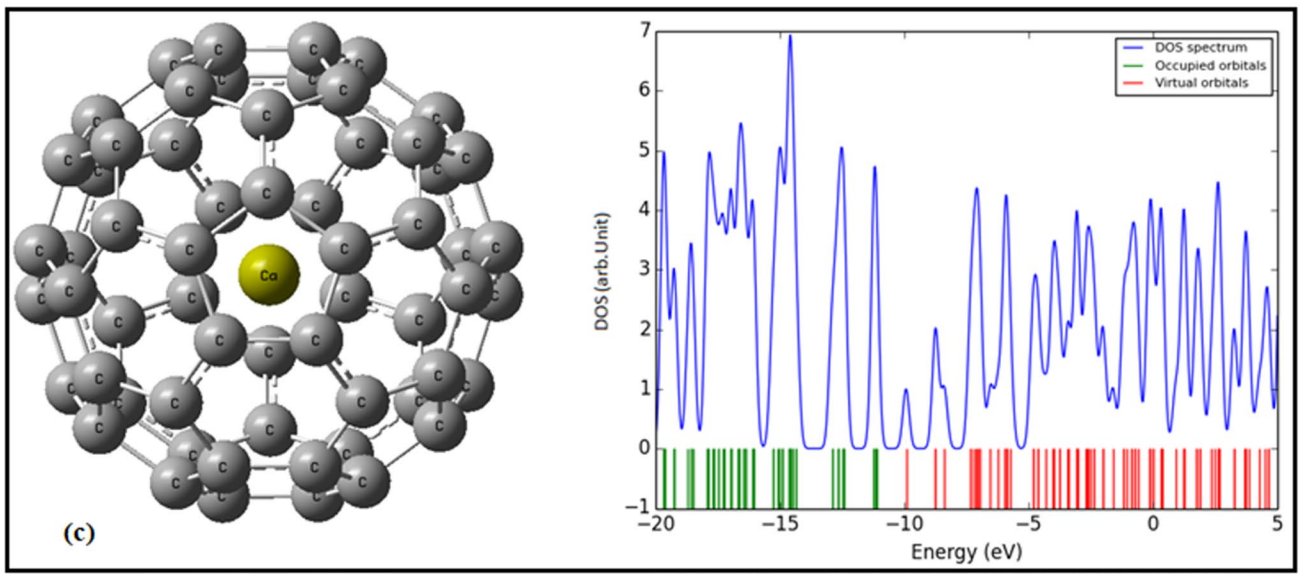
Ca
(c)
DOS spectrum
Occupied orbitals
Virtual orbitals
DOS (arb.Unit)
Energy (eV)

◂**Fig. 2** The optimized structures and DOS plots of fullerene C60 with divalent metal cations (M = Be^{2+}, Mg^{2+}, and Ca^{2+}) adsorbed at the center of a pentagon ring

adsorption process is chemisorption and the related nanocages are highly sensitive to divalent cations.

Electronic properties

Density of state (DOS) analysis is performed on the pristine C60 nanocage, SiC59, and the different M@C60 and M@SiC59 complexes to provide a comprehensive investigation of the effects of X-doping (X = Si) on the electronic structure and adsorption behavior of the metal cations on the C60 nanocages. As shown in Table 1, the energy gap value for the pristine C60 nanocage is equal to 2.76 eV, which means that it is a semiconductor material. The calculated DOS plots (Figs. 1, 2, and 3) exhibit that the electronic properties of the C60 and SiC59 nanocages significantly change with the addition of metal cations. According to the M@C60 and M@SiC59 DOS plots (Figs. 2 and 3), the E_g and Fermi level (E_{FL}, middle of the E_g at 0 K) of the alkaline earth complexes considerably change and shift toward lower energies. On the other hand, the results show that in the alkali complexes, E_g changes slightly downwards, which is negligible; thus, the DOS plots of alkali-adsorbed nanocages (plots not shown) are approximately close to the C60 and SiC59 nanocages.

The work function (ϕ) of a semiconductor can be calculated as the difference between the Fermi level energies and the vacuum level, which is the minimum energy required to separate one electron from the Fermi level to the infinite distance from the surface. The following equation indicates the calculated work function as:

$$\phi = E_{inf} - E_{FL} \tag{3}$$

where E_{inf} is the electrostatic potential at infinity (assumed to be zero) and E_{FL} is the Fermi level energy. In accordance with this guess, ϕ is equivalent to the negative amount of the Fermi level energy. It is obvious from Table 1 that the reduction in Fermi level is accompanied with the increment in work function. There is also a relationship between the emitted electron current density in vacuum (J) with the work function in exponential form (Richardson-Dushman equation), as given below:

$$J = AT^2 \exp(-\phi/kT) \tag{4}$$

According to this formula, A is the Richardson constant, T is the temperature, ϕ is the work function, and k is the Boltzmann constant. As can be seen, with increasing ϕ, the field emission properties (J) decrease. Hence, the work function is a major factor in evaluating the field electron emission.

The results of calculations also show that the adsorption of alkaline earth cations relative to the alkali ones in both the C60 and SiC59 nanocages leads to a significant increase in the work function and thus a noteworthy decrease in the emitted electron current density during the complexation. In fact, increasing the work function in these complexes can be attributed to the more charge transfer from the active sites of C60 and SiC59 nanocages to the alkaline earth cations compared to the alkali ones. Therefore, it can be concluded that adsorption of the alkaline earth cations may be more effective in evaluating the field emission properties of C60 and SiC59 nanocages.

In the DOS diagrams of the C60 and SiC59 nanocages containing alkaline earth cations compared to alkali cations, the valence level appreciably shifts to lower energies, which is in accordance with a significant reduction in their band gaps (see Figs. 2 and 3). This means that the selected nanocages are more sensitive to alkaline earth cations with respect to alkali ones; thus, the Fermi level for alkaline earth cations adsorbed on nanocages would diminish from − 4.60 and − 4.73 eV in C60 and SiC59 to − 11.16 and − 11.21 eV in Be^{2+}, − 11.24 and − 11.03 eV in Mg^{2+}, and − 10.51 and − 10.43 eV in Ca^{2+}, respectively.

The energy gap (E_g) is a major factor in determining the electrical conductivity of the materials, and a classic relation between them is as follows [63]:

$$\sigma \alpha \exp(-E_g/2kT) \tag{5}$$

where values of σ and k are the electric conductivity and the Boltzmann constant, respectively. It is clear that there is an inverse relationship between the energy gap values and their corresponding electrical conductivity. In other words, a decrease in E_g is associated with an increase in the electrical conductivity (σ) and vice versa. Table 1 presents the obtained values of E_g for the pristine C60 and SiC59 nanocages and their analogous complexes. By comparing the E_g values, it is found that after the adsorption of metal cations on the nanocages, the energy gaps in both systems change to some extent, so that these changes are more in the alkaline earth cations than in the alkali ones.

AIM analysis

The AIM theory allows one to study the concept of chemical bond and the bond strength in terms of the electron density distribution function [56, 64]. It exploits the topological features of electron density, $\rho(r)$, and thereby the definition of chemical bonding through the bond path and the bond critical point (BCP). The Laplacian of the electron density, $^2\rho(r)$, is also a measure of the local concentrations of electron density and may be positive or negative. The total

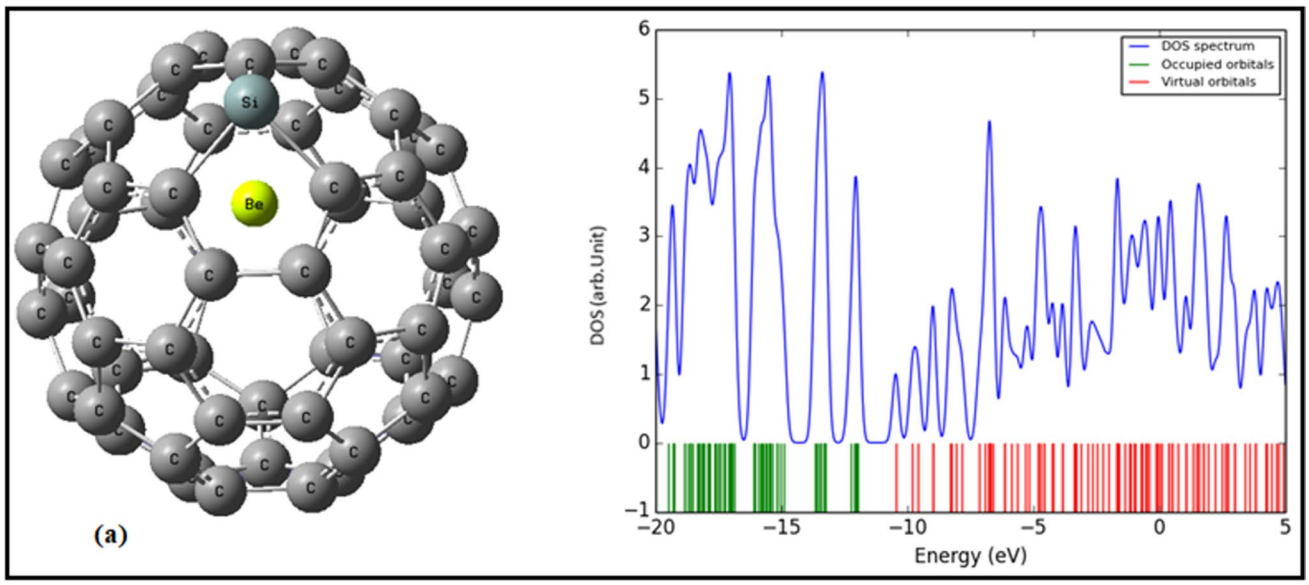
Si
Be
(a)
DOS spectrum
Occupied orbitals
Virtual orbitals
DOS (arb.Unit)
Energy (eV)

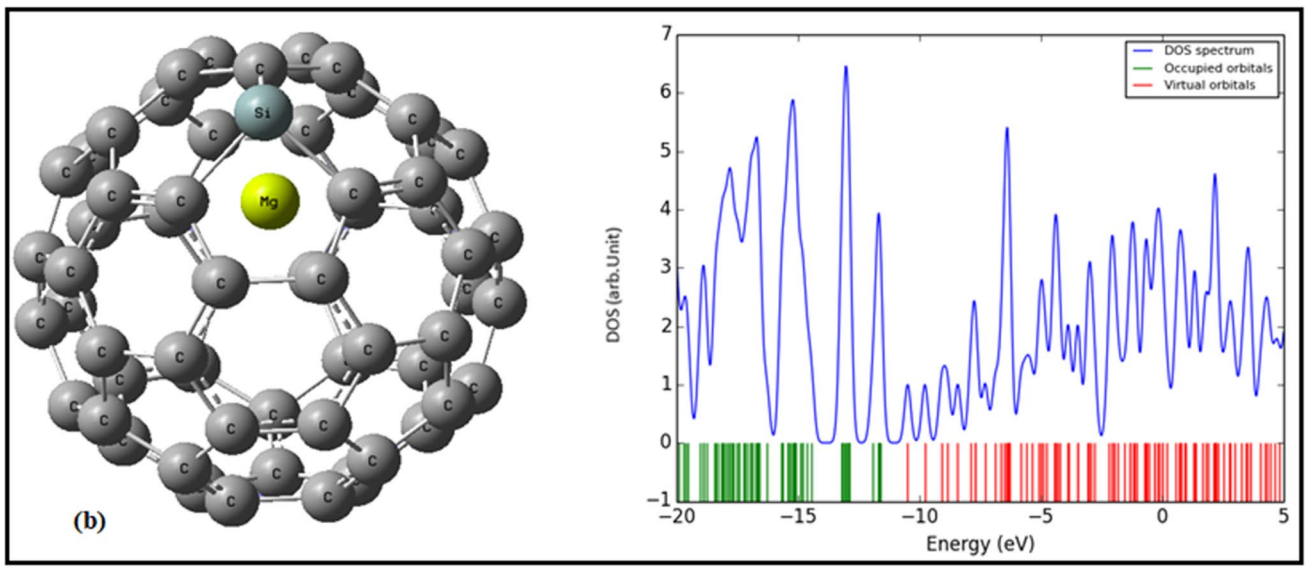
Si
Mg
(b)
DOS spectrum
Occupied orbitals
Virtual orbitals
DOS (arb.Unit)
Energy (eV)

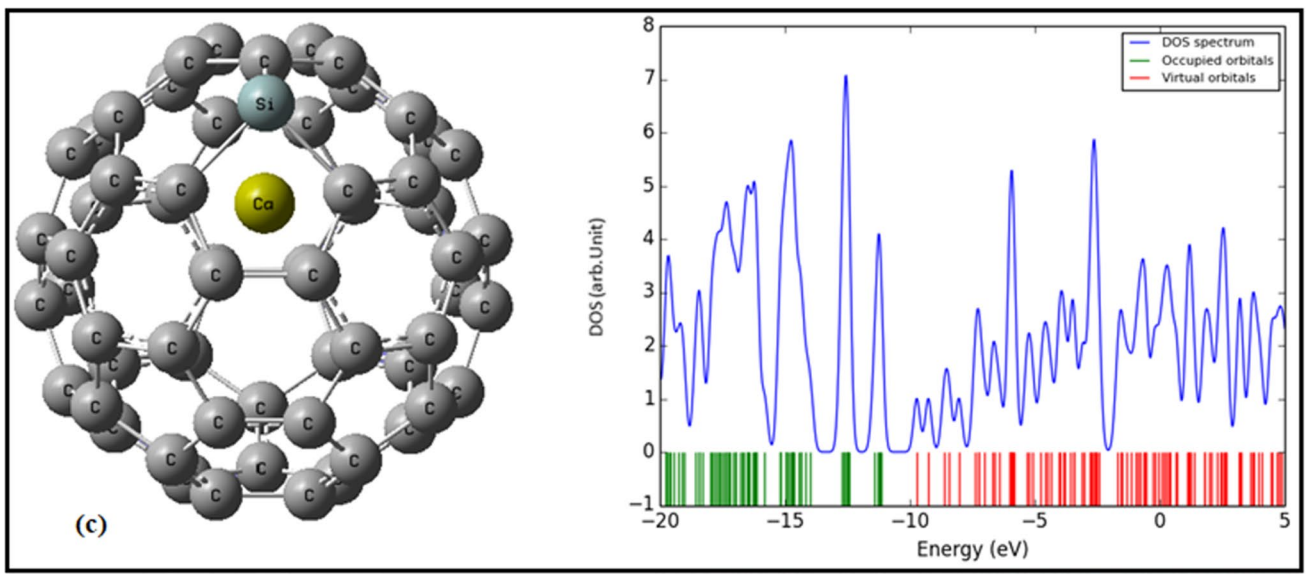
Si
Ca
(c)
DOS spectrum
Occupied orbitals
Virtual orbitals
DOS (arb.Unit)
Energy (eV)

◂**Fig. 3** The optimized structures and DOS plots of SiC59 with divalent metal cations (M = Be^{2+}, Mg^{2+}, and Ca^{2+}) adsorbed at the center of a pentagon ring

energy density in a BCP, $H(r)$, is another useful topological descriptor that provides supplementary information about the nature of the interactions.

A negative value of $^2\rho(r)$ (i.e., covalent interactions) denotes the electron concentration at a particular point, while a positive value of $^2\rho(r)$ (i.e., ionic interactions, van der Waals or hydrogen bonds) implies electron depletion [56]. The former interactions have a high value of the electron density in BCP of the order $> 10^{-1}$ a.u., and for the latter cases, the value of ρ is quite small ($\sim 10^{-2}$ a.u. or less). It has also been reported that if $^2\rho(r) > 0$ and $H(r) < 0$, this interaction is at least partly covalent in nature [65–68]. Figure 4 shows the typical molecular graphs obtained from AIM analysis for the Be^{2+}@C60 and Be^{2+}@SiC59 complexes.

The calculated topological parameters for the M@C60 and M@SiC59 complexes are shown in Table 2. As shown in this table, for all M@SiC59 complexes, the BCPs of interaction have low ρ, $^2\rho_{BCP} > 0$ and $H_{BCP} > 0$. These values indicate that the cation–π interaction in the studied complexes may be classified as the van der Waals interactions. However, in the Be^{2+} complex, the corresponding H_{BCP} value is negative, meaning that this interaction is at least partly covalent (see Table 2). It is also apparent from this table that the values of $\rho_{Si\cdots M}$ and $^2\rho_{Si\cdots M}$ for the divalent complexes are greater than the values of the monovalent. This denotes that the interaction between the divalent cations and SiC59 nanocage is stronger than the monovalent cations.

In the M@C60 complexes, the low $\rho_{C\cdots M}$ values and positive $^2\rho_{C\cdots M}$ also indicate a decrease in the electronic charge along the bond paths, which is specification of the van der Waals interactions (see Table 2). The interaction of the Be^{2+} complex is also the partially covalent in nature, due to the negative H_{BCP} in this compound. It is also observed that for each ion group (alkali metal and alkaline earth), with an increase in the cation size from up to down, the values of ρ_{BCP} and $^2\rho_{BCP}$ decrease as one goes from Be^{2+} (Li^+) to Mg^{2+} (Na^+) then to Ca^{2+} (K^+) (Table 2). For the analyzed complexes, this trend corresponds to a decrease in the cation–π interactions strength in each group.

NBO analysis

The NBO analysis [58] is achieved to provide a complete investigation of the adsorption behavior of the metal cations on the C60 and SiC59 nanocages. It is originally developed as a way to quantify the contribution of the resonance structure to molecules [69–77]. Table 3 shows the results of the NBO analysis including the second order perturbation interaction energy, $E^{(2)}$, and the occupation numbers of the donor and acceptor orbitals at the B3LYP/6-31G(d) level of theory. As shown in this Table, the charge transfer takes place from C60 and SiC59 nanocages to the alkali and alkaline cations. In other words, the dominant interaction in the analyzed complexes is between the σ-electrons of the donor species and an antibonding lone pair of the metal cations (σ → LP*). The result of calculations demonstrates that σ_{C-C} of the C60 and σ_{C-Si} of the SiC59 nanocages participate as donors and LP^*_{cation} acts as acceptor.

Based on the results of $E^{(2)}$ obtained from the NBO analysis, the interaction between cations with C60 and SiC59 nanocages decreases with an increase in the atomic number and the size of the metals cations from up to down (see Table 3). The order of $E^{(2)}$ in the M@SiC59 complexes is as $Be^{2+} > Mg^{2+} > Ca^{2+} \approx Li^+ > Na^+ > K^+$. Hence, the results confirm that the SiC59 surface has the stronger interaction with the alkaline earth cations with respect to the alkali ones; as a result, larger values of $E^{(2)}$ are associated with stronger donor–acceptor interactions and greater stability of the complexes [28].

Frontier molecular orbital analysis

Our final study in this paper is to evaluate the reactivity of C60s by analyzing their electronic structure. Figures 5 and 6 show the schematic diagrams of the HOMO and LUMO orbitals of the pristine C60, SiC59, and M@C60 and M@SiC59 complexes related to Be^{2+} as the most stable structure studied in this work. Table 1 shows variable information about quantum molecular descriptors such as softness (S), chemical hardness (η) [61], and electronegativity (χ) [62], which can be expressed as follows:

$$\eta = \frac{(E_{LUMO} - E_{HOMO})}{2} \tag{6}$$

$$\chi = \frac{-(E_{LUMO} + E_{HOMO})}{2} \tag{7}$$

$$S = \frac{1}{2\eta} \tag{8}$$

As can be seen, these parameters are computed using HOMO and LUMO energies (E_{HOMO} and E_{LUMO}) according to Koopman's theorem equations [78].

According to the principle of electronegativity equalization, formulated primarily by Sanderson [79–82], "when two or more atoms initially different in electronegativity are combined chemically, their electronegativities become equal in the molecule." In the studied complexes, due to different electronegativity and chemical hardness, the

Table 1 Adsorption energies of alkali and alkaline earth cations on C60 and SiC59 nanocages (E_{ads}, in eV), energies of HOMO and LUMO (in eV), gap energy (E_g, in eV), energy of Fermi level (E_{FL}, in eV), change of E_g upon adsorption of cations (ΔE (%)), work function (ϕ, in eV), electronegativity (χ, in eV), hardness (η, in eV), softness (S, in eV^{-1}), number of electrons transferred (ΔN), and dipole moment (μ, in debye)

	E_{ads}	E_{HOMO}	E_{FL}	E_{LUMO}	E_g	ΔE (%)	ΔN	ϕ	μ	χ	η	S
C60	—	-5.98	-4.60	-3.22	2.76	—	—	4.60	0.00	4.60	1.38	0.36
Li^+	−1.57	−8.73	−7.46	−6.19	2.53	−8.33	−0.516	7.46	11.06	7.46	1.27	0.79
Na^+	−1.07	−8.52	−7.23	−5.93	2.59	−6.16	−0.529	7.23	14.52	7.23	1.30	0.77
K^+	−0.66	−8.33	−7.01	−5.70	2.63	−4.71	−0.500	7.01	17.97	7.01	1.31	0.76
Be^{2+}	−12.07	−11.99	−11.16	−10.33	1.66	−39.86	−0.631	11.16	11.75	11.16	0.83	1.20
Mg^{2+}	−7.05	−11.57	−11.24	−10.91	0.66	−76.09	−0.723	11.24	18.88	11.24	0.33	3.04
Ca^{2+}	−4.28	−11.11	−10.51	−9.92	1.19	−56.88	−0.745	10.51	26.93	10.51	0.59	1.69
SiC59	—	−5.82	−4.73	−3.65	2.17	—	—	4.73	0.20	4.73	1.08	0.46
Li^+	−1.48	−8.68	−7.69	−6.69	1.98	−8.76	−0.519	7.69	10.68	7.69	0.99	1.01
Na^+	−1.04	−8.51	−7.51	−6.52	1.98	−8.76	−0.534	7.51	13.73	7.51	0.99	1.01
K^+	−0.64	−8.30	−7.28	−6.26	2.04	−5.99	−0.508	7.28	17.44	7.28	1.02	0.98
Be^{2+}	−12.25	−11.95	−11.21	−10.46	1.49	−31.34	−0.633	11.21	9.84	11.21	0.75	1.34
Mg^{2+}	−7.50	−11.59	−11.03	−10.48	1.12	−48.39	−0.729	11.03	15.80	11.03	0.56	1.79
Ca^{2+}	−4.47	−11.15	−10.43	−9.72	1.44	−33.64	−0.754	10.43	24.08	10.43	0.72	1.39

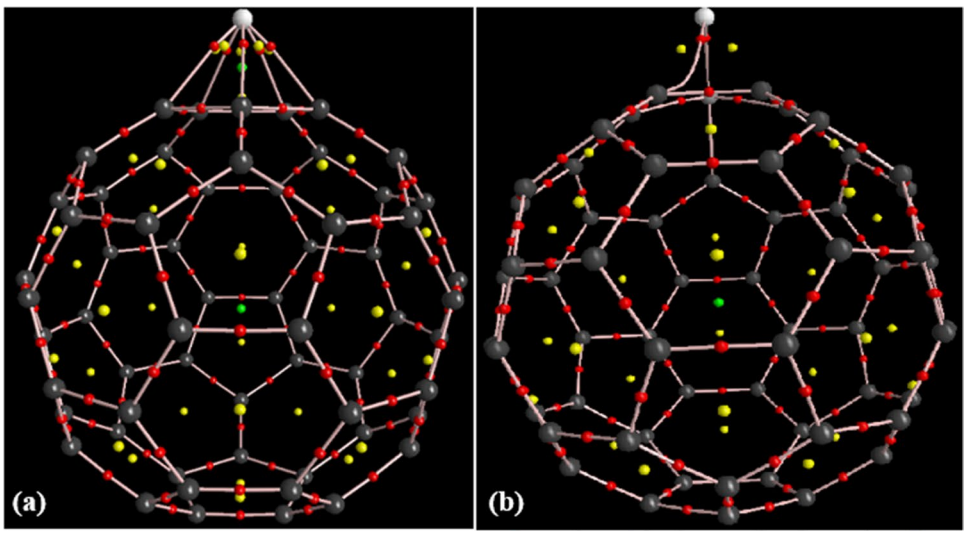

Fig. 4 The molecular graphs of **a** Be^{2+}@C60 and **b** Be^{2+}@SiC59 complexes obtained from the DFT calculation

Table 2 Topological parameters of the metal cations adsorbed on C60 and SiC59 nanocages (in a.u.)

C60				SiC59			
Bond	ρ_{BCP}	$^2\rho_{BCP}$	H_{BCP}	Bond	ρ_{BCP}	$^2\rho_{BCP}$	H_{BCP}
C•••Li^+	0.0154	0.0851	0.0044	Si•••Li^+	0.0105	0.0433	0.0022
C•••Na^+	0.0114	0.0556	0.0030	Si•••Na^+	0.0095	0.0353	0.0017
C•••K^+	0.0091	0.0369	0.0019	Si•••K^+	0.0067	0.0216	0.0011
C•••Be^{2+}	0.0588	0.2426	-0.0053	Si•••Be^{2+}	0.0530	0.0759	-0.0079
C•••Mg^{2+}	0.0286	0.1346	0.0035	Si•••Mg^{2+}	0.0311	0.0672	0.0015
C•••Ca^{2+}	0.0223	0.0920	0.0026	Si•••Ca^{2+}	0.0231	0.0532	0.0021

electron density flux is from that of with less χ to that with more χ. In other words, the electron is transferred to the lower electronic chemical potential, until the electronic chemical potentials become equal. Because, the electronegativity of Mulliken is characterized by the negative of electronic chemical potential ($\chi = -\mu$); thus, it must be constant everywhere. Hence, the values of χ and η obtained for calculating the number of electrons transferred (ΔN) from one system (nanocages) to another system (cations) [83] are applied as follows:

Table 3 NBO analysis of M@C60 and M@SiC59 complexes, occupation numbers of donor ($O.N._D$) and acceptor ($O.N._A$) orbitals and their energies (in kcal/mol) of some important orbitals

M^{n+}	Donor	$O.N._D$	Acceptor	$O.N._A$	$E^{(2)}$
Li^+	$\sigma_{C\text{-}C}$	1.9641	LP^*_{Li}	0.0180	1.09
Na^+	$\sigma_{C\text{-}C}$	1.9660	LP^*_{Na}	0.0149	0.44
K^+	$\sigma_{C\text{-}C}$	1.9650	LP^*_{K}	0.0023	0.22
Be^{2+}	$\sigma_{C\text{-}C}$	1.9345	LP^*_{Be}	0.0572	12.70
Mg^{2+}	$\sigma_{C\text{-}C}$	1.9609	LP^*_{Mg}	0.0122	2.20
Ca^{2+}	$\sigma_{C\text{-}C}$	1.9652	LP^*_{Ca}	0.0026	0.69
Li^+	$\sigma_{C\text{-}Si}$	1.9118	LP^*_{Li}	0.0219	0.85
Na^+	$\sigma_{C\text{-}Si}$	1.9191	LP^*_{Na}	0.0107	0.19
K^+	$\sigma_{C\text{-}Si}$	1.9222	LP^*_{K}	0.0026	0.07
Be^{2+}	$\sigma_{C\text{-}Si}$	1.8415	LP^*_{Be}	0.1069	28.40
Mg^{2+}	$\sigma_{C\text{-}Si}$	1.9186	LP^*_{Mg}	0.0224	3.52
Ca^{2+}	$\sigma_{C\text{-}Si}$	1.9057	LP^*_{Ca}	0.0060	0.85

$$\Delta N = \frac{1}{2}\frac{(\chi_{SiC59\text{or}C60} - \chi_M)}{(\eta_{SiC59\text{or}C60} + \eta_M)} \quad (9)$$

In this equation, $\chi_{\text{SiC59 or C60}}$, χ_M and $\eta_{\text{SiC59 or C60}}$, η_M are the electronegativity and chemical hardness of the SiC59 or pristine C60 nanocages and the M cations, respectively. A positive value of ΔN shows that charge flows from the cations to the nanocages and the nanocages act as electron acceptors, while a negative value of ΔN displays that charge flows from the nanocages to the cations and the nanocages act as electron donors. Table 1 shows the number of electrons transferred (ΔN) in the studied systems. As shown in table, the absolute values of ΔN in the divalent complexes are more than the monovalent ones. Hence, the electron-donating ability in the former cases is greater than the latter.

Another major electronic property that affects the selected complexes is the dipole moment (μ). Table 1 shows the dipole moment of the pristine C60 and SiC59 nanocages and their complexes computed by the DFT method. It is well known that the large dipole moments exhibit the high reactivity of molecules [84, 85]. In other words, the more

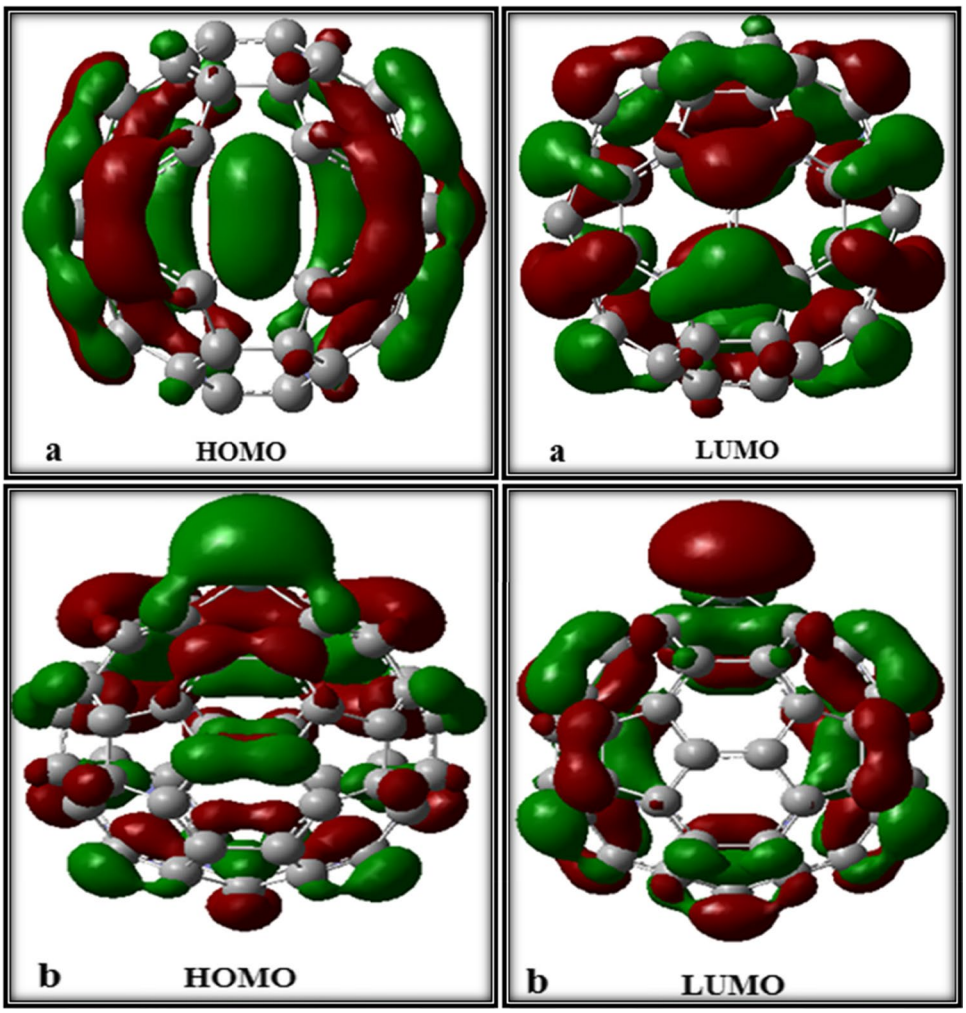

Fig. 5 The calculated orbitals localized at **a** HOMO and LUMO of isolated C60 **b** HOMO and LUMO of isolated SiC59

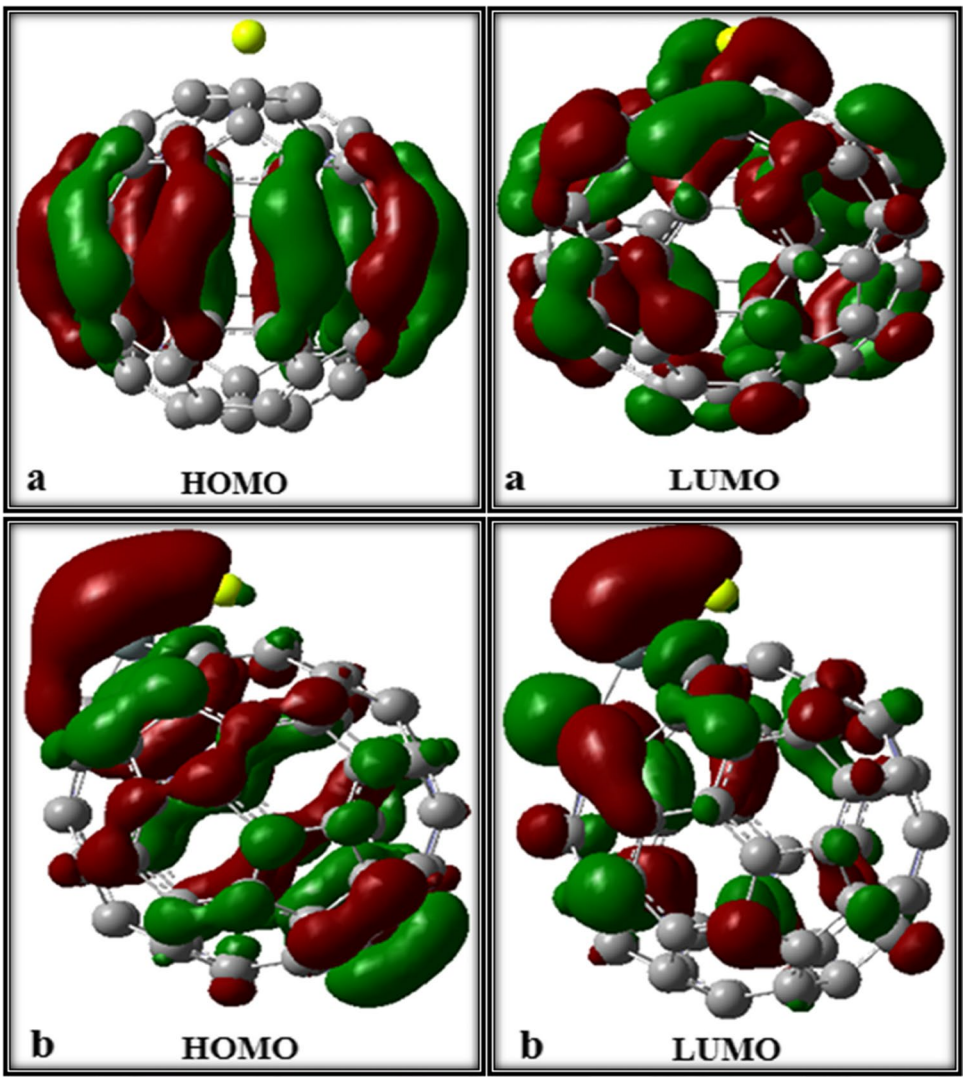

Fig. 6 The calculated orbitals localized at **a** HOMO and LUMO of the Be^{2+}@C60 complex and **b** HOMO and LUMO of the Be^{2+}@SiC59 complex

adsorption between adsorbent and adsorbate can be attributed to the high dipole moment in the compounds [86]. It can be noted that during the adsorption process of metal cations on the nanocage surface, depending on the adsorption configurations, the size and direction of the electric dipole moment vector change. The results shown in Table 1 display that in most cases, the highest dipole moments belong to divalent complexes and the lowest of those correspond to monovalent ones.

Conclusion

In the present study, the adsorption of alkali (Li^+, Na^+, K^+) and alkaline earth (Be^{2+}, Mg^{2+}, Ca^{2+}) cations on the pristine C60 and SiC59 nanocages as sensors with high electron donor is investigated, and their results are compared with together. The detection of these cations by the mentioned nanocages is considered by means of DFT calculations. From the obtained results, it can be understood that cations with a larger charge density interact more strongly with nanocages. The data show that the adsorption of alkaline earth cations on the SiC59 nanocage is stronger than the C60 one. The large values of E_{ads} denote that the adsorption process is chemisorption and the related nanocages are highly sensitive to divalent cations. The results of AIM analysis show that the investigated interactions in complexes are from type of the van der Waals. It is apparent that the values of ρ and $^2\rho$ for the divalent complexes are higher than those of the monovalent ones. This denotes that the interaction between the divalent cations and nanocages is stronger than the monovalent cations. The NBO analysis also shows that the SiC59 surface has the stronger interaction with the alkaline earth cations with respect to the alkali ones; hence, larger values of $E^{(2)}$ are associated with stronger donor–acceptor interactions and greater stability of the complexes. The calculated DOS plots show that the E_g and Fermi levels of the alkaline earth complexes considerably change and shift toward lower

energies, while in the alkali complexes, E_g changes slightly downwards, which is negligible and approximately close to the selected nanocages. The results of calculations also show that the adsorption of alkaline earth cations relative to the alkali ones in both the C60 and SiC59 nanocages leads to a significant increase in the work function and thus a noteworthy decrease in the emitted electron current density during the complexation. By comparing the E_g values, it is found that after the adsorption of metal cations on the nanocages, the energy gaps in both systems change to some extent, so that these changes are more in the alkaline earth cations than in the alkali ones. Thus, the nanocages used in this study could be interest sensors for the detection of the alkaline earth cations.

Acknowledgements The authors wish to thank from Payame Noor University, Tehran, Iran, for their supports.

Author contribution All the authors have accepted responsibility for the entire content of this submitted manuscript and approved submission.

Data availability All data generated or analyzed during this study are included in this article.

Code availability Not applicable.

Declarations

Ethics approval The manuscript is prepared in compliance with the Ethics in Publishing Policy as described in the Guide for Authors.

Consent to participate The manuscript is approved by all authors for publication.

Consent for publication The consent for publication was obtained from all participants.

Conflict of interest The authors declare no competing interests.

References

1. Kroto W, Heath JR, O'Brien SC, Curl RF, Smalley RE (1985) C60: buckminsterfullerene. Nature 318:162–163
2. Zahedi E (2013) Adsorption of nitrogen dioxide on $C_{30}B_{15}N_{15}$ heterofullerene: AIM and NBO study via DFT. C R Chimie 16:189–194
3. Lalwani G, Sitharaman B (2013) Multifunctional fullerene and metallofullerene based nanobiomaterials. Nano LIFE 3:1342003
4. Yang M, Li C, Zhang Y, Jia D, Zhang X, Hou Y, Li R, Wang J (2017) Maximum undeformed equivalent chip thickness for ductile-brittle transition of zirconia ceramics under different lubrication conditions. Int J Mach Tools Manuf 122:55–65
5. Yang M, Li C, Zhang Y, Jia D, Li R, Hou Y, Cao H, Wang J (2019) Predictive model for minimum chip thickness and size effect in single diamond grain grinding of zirconia ceramics under different lubricating conditions. Ceram 45(12):14908–14920
6. Zhang Y, Li HN, Li C, Huang C, Ali HM, XU X, Mao C, Ding W, Cui X, Yang M, Yu T, Jamil M, Gupta MK, Jia D, Said Z (2022) Nano-enhanced biolubricant in sustainable manufacturing: from processability to mechanisms. Friction 10:803–841
7. Li B, Li C, Zhang Y, Wang Y, Jia D, Yang M (2016) Grinding temperature and energy ratio coefficient in MQL grinding of high-temperature nickel-base alloy by using different vegetable oils as base oil. Chinese J Aeronaut 29(4):1084–1095
8. Guo S, Li C, Zhang Y, Wang Y, Li B, Yang M, Zhang X, Liu G (2017) Experimental evaluation of the lubrication performance of mixtures of castor oil with other vegetable oils in MQL grinding of nickel-based alloy. J Clean Prod 140:1060–1076
9. Zhang J, Li C, Zhang Y, Yang M, Jia D, Liu G, Hou Y, Li R, Zhang N, Wu Q, Cao H (2018) Experimental assessment of an environmentally friendly grinding process using nanofluid minimum quantity lubrication with cryogenic air. J Clean Prod 193:236–248
10. Rutherglen C, Jain D, Burke P (2009) Nanotube electronics for radiofrequency applications. Nat Nanotechnol 4:811–819
11. Schwierz F (2010) Graphene transistors. Nat Nanotechnol 5:487–496
12. Motaung DE, Malgas GF, Arendse CJ (2011) Insights into the stability and thermal degradation of P3HT: C60 blended films for solar cell applications. J Mater Sci 46:4942–4952
13. Haddon R (1992) Electronic structure, conductivity and superconductivity of alkali metal doped (C60). Acc Chem Res 25:127–133
14. Vessally E, Farajzadeh P, Najafi E (2021) Possible sensing ability of boron nitride nanosheet and its Al– and Si–doped derivatives for methimazole drug by computational study. Iran J Chem Chem Eng 40:1001–1011
15. Vessally E, Musavi M, Poor Heravi MR (2021) A density functional theory study of adsorption ethionamide on the surface of the pristine, Si and Ga and Al-doped graphene. Iran J Chem Eng (IJCCE) 40 in Press
16. Vessally E, Hosseinian A (2021) A computational study on some small graphene-like nanostructures as the anodes in Na−ion Batteries. Iran J Chem Chem Eng 40:691–703
17. Gharibzadeh F, Vessally E, Edjlali L, Es'haghi M, Mohammadi R (2020) A DFT study on sumanene, corannulene and nanosheet as the anodes in Li−Ion batteries. Iran J Chem Chem Eng 39:51-62
18. Hashemzadeh B, Edjlali L, Delir Kheirollahi Nezhad P, Vessally E (2021) A DFT studies on a potential anode compound for Li-ion batteries: hexa-cata-hexabenzocoronene nanographen. Chem Rev Lett 4:232–238
19. Bosi S, Da Ros T, Castellano S, Banfi E, Prato M (2000) Antimycobacterial activity of ionic fullerene derivatives. Bioorg Med Chem Lett 10:1043–1045
20. Friedman SH, DeCamp DL, Sijbesma RP, Srdanov G, Wudl F, Kenyon GL (1993) Inhibition of the HIV-1 protease by fullerene derivatives: model building studies and experimental verification. J Am Chem Soc 115:6506–6509
21. Nakamura E, Tokuyama H, Yamago S, Shiraki T, Sugiura Y (1996) Biological activity of water-soluble fullerenes. Structural dependence of DNA cleavage, cytotoxicity, and enzyme inhibitory activities including HIV-protease inhibition. Bull Chem Soc Jpn 69:2143–2151
22. Luo B, Liu G, Wang L (2016) Recent advances in 2D materials for photocatalysis. Nanoscale 8:6904–6920
23. Novoselov KS, Geim AK, Morozov SV, Jiang D, Zhang Y, Dubonos SV, Grigorieva IV, Firsov AA (2004) Electric field in atomically thin carbon films. Science 306:666–669
24. Chen M, Guan R, Yang S (2019) Hybrids of fullerenes and 2D nanomaterials. Adv Sci (Weinh) 6:1800941
25. Jalali Sarvestani MR, Charehjou P (2021) Fullerene (C_{20}) as a potential adsorbent and sensor for the removal and detection of

picric acid contaminant: a DFT Study. Cent Asian J Environ Sci Technol Innov 2(1):12–19
26. Onur Uygun Z, Ertuğrul Uygun HD (2020) Fullerene based sensor and biosensor technologies, In book: Nanosystems, IntechOpen
27. Ren XY, Jiang CY (2012) Density functional studies on the endohedral complex of fullerene C70 with tetrahedrane (C_4H_4): C_4H_4@C70. J Mol Model 18:3213–3217
28. Alipour Zaghmarzi F, Zahedi M, Mola A, Abedini S, Arshadi S, Ahmadzadeh S, Etminan N, Younesi O, Rahmanifar E, Yoosefian M (2017) Fullerene-C60 and crown ether doped on C60 sensors for high sensitive detection of alkali and alkaline earth cations. Physica E 87:51–58
29. Zheng J, Ren Z, Guo P, Fang L, Fan J (2011) Diffusion of Li^+ ion on graphene: a DFT study. Appl Surf Sci 258:1651–1655
30. Sanghavi BJ, Varhue W, Rohani A, Liao KT, Bazydlo LA, Chou CF, Swami NS (2015) Ultrafast immunoassays by coupling dielectrophoretic biomarker enrichment in nanoslit channel with electrochemical detection on graphene. Lab Chip 15:4563–4570
31. Sanghavi BJ, Moore JA, Chávez JL, Hagen JA, Kelley-Loughnane N, Chou CF, Swami NS (2016) Aptamer-functionalized nanoparticles for surface immobilization-free electrochemical detection of cortisol in a microfluidic device. Biosens Bioelectron 78:244–252
32. Sanghavi BJ, Varhue W, Chávez JL, Chou CF, Swami NS (2014) Electrokinetic preconcentration and detection of neuropeptides at patterned graphene-modified electrodes in a nanochannel. Anal Chem 86:4120–4125
33. Zhang X, Tang Y, Zhang F, Lee C (2016) A novel aluminum-graphite dual-ion battery. Adv Energy Mater 6(11):1502588
34. Tong X, Zhang F, Ji B, Sheng M, Tang Y (2016) carbon-coated porous aluminum foil anode for high-rate, long-term cycling stability, and high energy density dual-ion batteries. Adv Mater (Weinh) 28(45):9979–9985
35. Ji B, Zhang F, Song X, Tang Y (2017) A novel potassium-ion-based dual-ion battery. Adv Mater (Weinh) 29(19):1700519
36. Wang M, Jiang C, Zhang S, Song X, Tang Y, Cheng HM (2018) Reversible calcium alloying enables a practical room-temperature rechargeable calcium-ion battery with a high discharge voltage. Nat Chem 10(6):667–672
37. Jiang L, Wang Y, Wang X, Ning F, Wen S, Zhou Y, Chen S, Betts A, Jerrams S, Zhou F (2021) Electrohydrodynamic printing of a dielectric elastomer actuator and its application in tunable lenses. Compos-A: Appl Sci Manuf 147:106461
38. Li T, Yin W, Gao S, Sun Y, Xu P, Wu S, Kong H, Yang G, Wei G (2022) The combination of two-dimensional nanomaterials with metal oxide nanoparticles for gas sensors: a review. Nanomaterials 12(6):982
39. Yan H, Zhao M, Feng X, Zhao S, Zhou X, Li S, Zha M, Meng F, Chen X, Liu Y, Chen D, Yan N, Yang C (2022) PO_4^{3-} coordinated robust single-atom platinum catalyst for selective polyol oxidation. Angew Chem Int Ed e202116059
40. Zhang R, Zhang W, Shi M, Li H, Ma L, Niu H (2022) Morphology controllable synthesis of heteroatoms-doped carbon materials for high-performance flexible supercapacitor. Dyes Pigm 199:109968
41. Huang Z, Luo P, Zheng H (2022) Design of Ti^{4+}-doped $Li_3V_2(PO_4)_3$/C fibers for lithium energy storage. Ceram 48(6):8325–8330
42. Becke AD (1993) Density-functional thermochemistry. III. The role of exact exchange. J Chem Phys 98:5648–5652
43. Lee C, Yang W, Parr RG (1998) Development of the Colle-Salvetti correlation-energy formula into a functional of the electron density. Phys Rev B 37:785–789
44. Ahmadi A, Hadipour NL, Kamfiroozi M, Bagheri Z (2012) Theoretical study of aluminum nitride nanotubes for chemical sensing of formaldehyde. Sens Actuators B Chem 161:1025–1029
45. Beheshtian J, Kamfiroozi M, Bagheri Z, Ahmadi A (2012) Theoretical study of hydrogen adsorption on the $B_{12}P_{12}$ fullerene-like nanocluster. Comput Mater Sci 54:115–118
46. Eid KM, Ammr HY (2011) Adsorption of SO_2 on Li atoms deposited on MgO (1 0 0) surface: DFT calculations. Appl Surf Sci 257:6049–6058
47. Dinadayalane TC, Murray JS, Concha MC, Politzer P, Leszczynski J (2010) Reactivities of sites on (5, 5) single-walled carbon nanotubes with and without a Stone-Wales defect. J Chem Theory Comput 6:1351–1357
48. Zhao TH, Castillo O, Jahanshahi H, Yusuf A, Alassafi MO, Alsaadi FE, Chu YM (2021) A fuzzy-based strategy to suppress the novel coronavirus (2019-NCOV) massive outbreak. Appl Comput Math 20(1):160–176
49. Zhao TH, Wang MK, Hai GJ, Chu YM (2022) Landen inequalities for Gaussian hypergeometric function. Revista de la Real Academia de Ciencias Exactas, Físicas y Naturales. Serie A. Matemáticas 116(1):1–23
50. Nazeer M, Hussain F, Ijaz Khan M, Asad-ur-Rehman E-Z, Chu YM, Malik MY (2021) Theoretical study of MHD electro-osmotically flow of third-grade fluid in micro channel. Appl Math Comput 420:126868
51. Zhao TH, Khan MI, Chu YM (2021) Artificial neural networking (ANN) analysis for heat and entropy generation in flow of non-Newtonian fluid between two rotating disks. Math Methods Appl Sci
52. Zhao TH, Wang MK, Zhang W (2018) Chu YM (2018) Quadratic transformation inequalities for Gaussian hypergeometric function. J Inequal Appl 1:251–266
53. Chu YM, Nazir U, Sohail M, Selim MM, Lee JR (2021) Enhancement in thermal energy and solute particles using hybrid nanoparticles by engaging activation energy and chemical reaction over a parabolic surface via finite element approach. Fractal Fract 5(3):119–136
54. Schmidt MW, Baldridge KK, Boatz JA, Elbert ST, Gordon MS, Jensen JH, Koseki S, Matsunaga N, Nguyen KA, Su SJ, Windus TL, Dupuis M, Montgomery JA (1993) General atomic and molecular electronic structure system. J Comput Chem 14:1347–1363
55. Boys SF, Bernardi F (1970) The calculation of small molecular interactions by the differences of separate total energies. Some procedures with reduced errors. Mol Phys 19:553–566
56. Bader RFW (1990) Atoms in molecules: a quantum theory. Clarendon, Oxford
57. BieglerKönig F, Schönbohm J (2002) Update of the AIM2000-program for atoms in molecules. J Comput Chem 23:1489–1494
58. Foster JP, Weinhold F (1980) Natural hybrid orbitals. J Am Chem Soc 102:7211–7218
59. Paul BK, Mahanta S, Singh RB, Guchhait N (2010) A DFT-based theoretical study on the photophysics of 4-hydroxyacridine: single-water-mediated excited state proton transfer. J Phys Chem A 114:2618–2627
60. O'Boyle N, Tenderholt A, Langner K (2008) cclib: a library for package-independent computational chemistry algorithms. J Comput Chem 29:839–845
61. Pearson RG (1997) Chemical Hardness. Wiley-VCH, Oxford
62. Sen KD, Jorgensen CK (1987) Electronegativity, structure and bonding. Springer-Verlag, New York
63. Li S (2006) Semiconductor physical electronics, 2nd edn. Springer, USA
64. Bader RFW (1998) A bond path: a universal indicator of bonded interactions. J Phys Chem A 102:7314–7323
65. Pacios LF (2004) Topological descriptors of the electron density and the electron localization function in hydrogen bond dimers at short intermonomer distances. J Phys Chem A 108:1177–1188

66. Jenkins S, Morrison I (2000) The chemical character of the intermolecular bonds of seven phases of ice as revealed by ab initio calculation of electron densities. Chem Phys Lett 317:97–102
67. Arnold WD, Oldfield E (2000) The chemical nature of hydrogen bonding in proteins via NMR: J-couplings, chemical shifts, and AIM theory. J Am Chem Soc 122:12835–12841
68. Rozas I, Alkorta I, Elguero J (2000) Behavior of ylides containing N, O, and C atoms as hydrogen bond acceptors. J Am Chem Soc 122:11154–11161
69. Linares M, Humbel S, Braïda B (2007) Quantifying resonance through a Lewis Valence Bond approach: application to haloallyl and carbonylcations. Faraday Discuss RSC 135:273–283
70. Salehi N, Vessally E, Edjlali L, Alkorta I, Eshaghi M (2020) Nan@Tetracyanoethylene (n=1-4) systems: sodium salt vs sodium electride. Chem Rev Lett 3:207–217
71. Sreerama L, Vessally E, Behmagham F (2020) Oxidative lactamization of amino alcohols: an overview. J Chem Lett 1:9–18
72. Majedi S, Sreerama L, Vessally E, Behmagham F (2020) Metal-free regioselective thiocyanation of (hetero) aromatic C-H bonds using ammonium thiocyanate: an overview. J Chem Lett 1:25–31
73. Ahmadi R, Kalateh K, Alizadeh R, Khoshtarkib Z, Amani V (2009) Tetra-kis(6-methyl-2,2′-bipyridine)-12 N, N′2 2 N, N′32 N, N′42 N, N′-tetra-nitrato-1:22 O:O′2:33 O:O′, O′′2: 33 O, O′:O′′3:42 O:O′-tetra-nitrato-14 O, O′42 O, O′-tetra-lead(II). Acta Crystallogr E 65:m1169–m1170
74. Soleimani-Amiri S, Asadbeigi N, Badragheh S (2020) A theoretical approach to new triplet and quintet (nitrenoethynyl) alkylmethylenes, (nitrenoethynyl) alkylsilylenes, (nitrenoethynyl) alkylgermylenes. Iran J Chem Chem Eng (IJCCE) 39(4):39–52
75. Norouzi N, Ebadi AG, Bozorgian A, Vessally E, Hoseyni SJ (2021) Energy and exergy analysis of internal combustion engine performance of spark ignition for gasoline, methane, and hydrogen fuels. Iran J Chem Chem Eng (IJCCE) 40⁦ in Press
76. Ma X, Kexin Z, Yonggang W, Ebadi AG, Toughani M (2021) Investigation of low-temperature lipase production and enzymatic properties of Aspergillus Niger. Iran J Chem Chem Eng (IJCCE) 40(4):1364–1374
77. Vessally E, Mohammadi S, Abdoli M, Hosseinian A, Ojaghloo P (2020) Convenient and robust metal-free synthesis of benzazole-2-ones through the reaction of aniline derivatives and sodium cyanate in aqueous medium. Iran J Chem Chem Eng (IJCCE) 39(5):11–19
78. Koopmans T (1934) Über die Zuordnung von Wellenfunktionen und Eigenwerten zu den Einzelnen Elektronen Eines Atoms. Physica 1:104–113
79. Sanderson RT (1955) Partial charges on atoms in organic compounds. Science 121:207–208
80. Sanderson RT (1976) Chemical bonds and bond energy, 2nd edn. Academic Press, New York
81. Chattaraj PK, Lee H, Parr RG (1991) DFT-based quantitative prediction of regioselectivity: cycloaddition of nitrilimines to methyl propiolate. J Am Chem Soc 113:1855–1856
82. Gázquez JL (1993) In Chemical hardness. Springer-Verlag, Berlin, Germany
83. Parr RG, Pearson RG (1983) Absolute hardness: companion parameter to absolute electronegativity. J Am Chem Soc 105:7512–7516
84. Sridevi C, Shanthi G, Velraj G (2012) Structural, vibrational, electronic, NMR and reactivity analyses of 2-amino-4H-chromene3-carbonitrile (ACC) by ab initio HF and DFT calculations. Spectrochim Acta A Mol Biomol Spectrosc 89:46–54
85. Raissi H, Khanmohammadi A, Mollania F (2013) A theoretical DFT study on the structural parameters and intramolecular hydrogen-bond strength in substituted (Z)-N-(thionitrosomethylene) thiohydroxylamine systems. Bull Chem Soc Jpn 86:1261–1271
86. Li X, Deng S, Fu H, Li T (2009) Adsorption and inhibition effect of 6-benzylaminopurine on cold rolled steel in 1.0 M HCl. Electrochim Acta 54:4089–4098

Publisher's note Springer Nature remains neutral with regard to jurisdictional claims in published maps and institutional affiliations.